



AAA-ATPase valosin-containing protein binds the transcription factor SREBP1 and promotes its proteolytic activation by rhomboid protease RHBDL4

Received for publication, February 16, 2022, and in revised form, March 29, 2022. Published, Papers in Press, April 14, 2022.
<https://doi.org/10.1016/j.jbc.2022.101936>

Koji Shibuya, Ken Ebihara^{*}, Chihiro Ebihara, Nagisa Sawayama, Masayo Isoda, Daisuke Yamamuro, Manabu Takahashi, Shuichi Nagashima, and Shun Ishibashi

From the Division of Endocrinology and Metabolism, Department of Internal Medicine, Jichi Medical University School of Medicine, Shimotsuke, Tochigi, Japan

Edited by George DeMartino

Valosin-containing protein (VCP) is a member of AAA-ATPase superfamily involved in various cellular functions. To investigate the pathophysiological role of VCP in metabolic disorders, we generated knock-in mice bearing an A232E mutation in VCP, a known human VCP pathogenic variant. When heterozygous mutant mice (A232E/+) were fed a high-fat diet, we observed that fatty liver was ameliorated and the proteolytic processing of the transcription factor sterol regulatory element-binding protein 1 (SREBP1) was impaired. Further co-immunoprecipitation analysis in wildtype mice revealed interactions of VCP with SREBP1 and a rhomboid protease, RHBDL4, in the liver, and these interactions were attenuated in A232E/+ mice. Consistent with these results, we show that knockdown or chemical inhibition of VCP or RHBDL4 in human hepatocytes impaired the proteolytic processing of SREBP1. Finally, we found that knockdown of E3 ligases such as glycoprotein 78 and HMG-CoA reductase degradation protein 1 disrupted the interaction of VCP with SREBP1 and impaired the proteolytic processing of SREBP1. These results suggest that VCP recognizes ubiquitinated SREBP1 and recruits it to RHBDL4 to promote its proteolytic processing. The present study reveals a novel proteolytic processing pathway of SREBP1 and may lead to development of new therapeutic strategies to treat fatty liver diseases.

Nonalcoholic fatty liver disease (NAFLD) is characterized by excessive accumulation of hepatic triglycerides (TGs) and hyperglycemia due to insulin resistance and is a hepatic component of metabolic syndrome (1). It can progress to liver cirrhosis, and sometimes to hepatocellular carcinoma (2). The prevalence rate is estimated to be approximately 25% of adults globally and is increasing worldwide (3, 4). Although many drugs have been investigated to date, there is no established therapy for NAFLD. Therefore, development of new treatments for NAFLD is the issue to be solved. Increased fatty acid synthesis in the liver is one of the major causes of NAFLD (5). Expressions of genes related to fatty acid synthesis are

positively regulated by sterol regulatory element-binding protein 1 (SREBP1), especially SREBP1c in the liver (6). So, SREBP1c can be a target of novel treatments for NAFLD. Indeed, polyunsaturated fatty acids have been shown to improve dyslipidemia by targeting SREBP1 (7).

The SREBP family is composed of two SREBP1 splice variants, SREBP1a and SREBP1c, and SREBP2 (8). SREBP1 mainly increases transcription of genes involved in fatty acid and TG synthesis, while SREBP2 primarily targets genes in the cholesterol biosynthetic pathway (8). SREBPs bind to SREBP cleavage-activating protein (SCAP) in the endoplasmic reticulum (ER) and are transported to the Golgi apparatus to be cleaved by site-1 protease (S1P) and site-2 protease (S2P) (8). It is well known that SREBP1 is regulated by fatty acids and insulin through feedforward control, whereas SREBP2 is controlled by sterols that regulate the binding between SCAP and insulin-induced gene (INSIG) through negative feedback (9). However, there are still many unknowns about the activation mechanism of SREBPs. Interestingly, in *Drosophila* which is completely lacking *dscap*, dSREBP still can be cleaved (10). This suggests the existence of the other SREBP activation mechanism in which SCAP is not involved.

Valosin-containing protein (VCP) is a hexameric protein belonging to the AAA (ATPase associated with various cellular activities) ATPase family (11). VCP is involved in many cellular functions, such as ER-associated degradation (ERAD), proteasome-mediated protein degradation, and lysosomal protein degradation (12). Gain-of-function mutations in VCP have been reported to cause inclusion body myopathy associated with Paget's disease of bone and frontotemporal dementia or multisystem proteinopathy (11, 13). ER stress associates with various diseases. Inhibition of ATPase activity of VCP without affecting other cellular functions of VCP leads to elicit neuroprotective effects in mouse models of glaucoma, retinitis pigmentosa, and Parkinson's disease and cardioprotective effects in a murine myocardial infarction model (12, 14–16). It is also well known that ER stress is involved in metabolic diseases such as diabetes mellitus and obesity (17–20). However, pathophysiological significance of VCP in

^{*} For correspondence: Ken Ebihara, kebihara@jichi.ac.jp.

VCP and proteolytic processing of SREBP1

these metabolic disorders is unclear. Therefore, in order to investigate it, we generated VCP A232E knock-in mice using a CRISPR/Cas9 system. A232E is one of human VCP pathogenic mutations that have been shown to cause multisystem pro- teinopathy (11, 21).

Since homozygous A232E (A232E/A232E) mice died within a few days after birth, we analyzed using heterozygous A232E (A232E/+) mice in the present study. When mice were fed high-fat diet (HFD), diet-induced fatty liver was ameliorated, but intra-abdominal fat mass was enlarged in A232E/+ mice. We also found that the processing of SREBP1 in the liver was impaired. Since no decrease in ATP concentration or no change in ER stress was observed in the liver of young A232E/+ mice used in the present study, it was suggested that the alteration in ATPase activity of VCP did not affect the processing of SREBP1.

Previous studies in yeast showed that Rbd2, a rhomboid protease in yeast, is required for SREBP activation; Cdc48, a yeast homolog of mammalian VCP, binds to Rbd2; and inhibition of this binding impairs SREBP processing (22–24). Moreover, in yeast, defective for SREBP cleavage (Dsc) E3 ubiquitin ligase acts on SREBP prior to the cleavage by Rbd2 (23). Cdc48 acts to recruit ubiquitinated substrates (23). Since it has been demonstrated that RHBDL4, a mammalian rhomboid protease, interacts with VCP during ERAD (25), we hypothesized that VCP facilitates the cleavage of SREBP1 by recruiting RHBDL4 to SREBP1 in murine liver.

The present study revealed a novel proteolytic processing pathway of SREBP1 in which VCP plays an essential role in murine liver and human hepatocytes. Elucidation of novel mechanism of SREBP1 activation may lead to the development of new therapeutic methods for fatty liver.

Results

Generation of A232E/+ mice and their growth curve

VCP is composed of four domains: the N-terminal domain, two ATPase domains (D1 and D2) with the linker regions on their N-terminal sides (L1 and L2), and the C-terminal domain (26). VCP is 100% identical at the amino acid level between mouse and human (27). The pathogenic A232E missense mutation is located in the D1 ATPase domain (Fig. 1A). We generated a *Vcp*^{A232E} missense mouse model using the CRISPR/Cas9 system. The *Vcp*^{A232E} allele carries the desired missense mutation that results in an A-to-E conversion, a *Dra* I restriction enzyme cut site, and an additional silent mutation to prevent Cas9 activity in the repaired allele (Fig. 1B). Transmission of the mutant allele was verified by PCR amplification and sequencing to confirm the presence of both the *Vcp*^{A232E} mutation and *Dra* I site at the appropriate locations (Fig. 1C). Routine genotyping of animals took advantage of the *Dra* I site to distinguish between wildtype (WT), heterozygous, and homozygous mutant animals (Fig. 1D). Restriction digestion of the 775-bp PCR product of the mutant

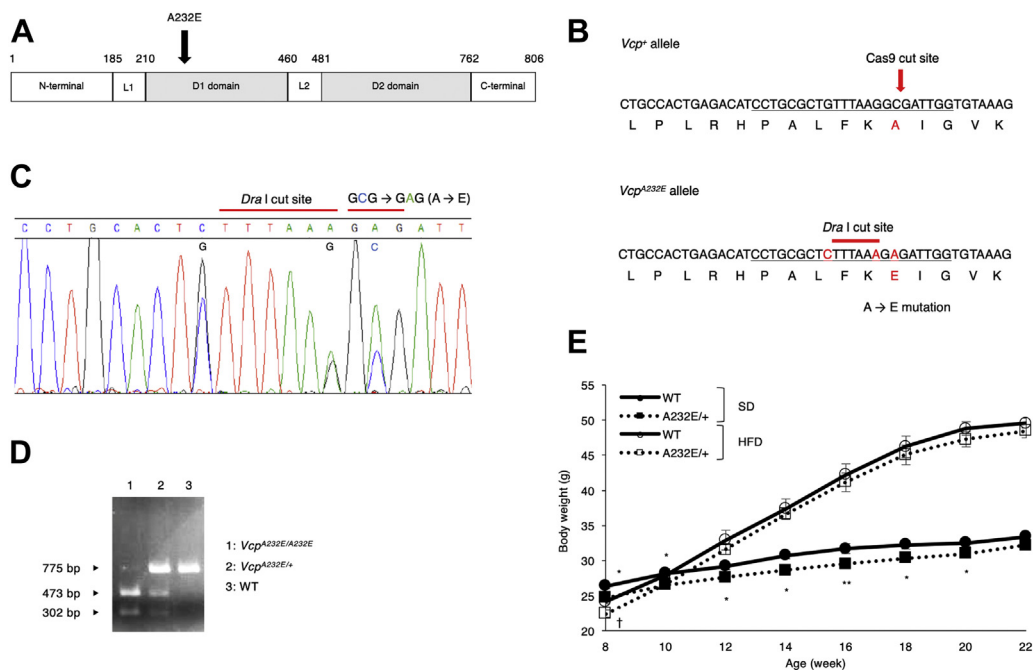


Figure 1. Generation of A232E mouse using CRISPR/Cas9. A, schematic domain organization of mouse and human VCP proteins those are 100% identical at the amino acid level. A232E mutation is located in the D1 ATPase domain. B, nucleotide sequences of *Vcp*⁺ and *Vcp*^{A232E} alleles around the A232E mutation. CRISPR target is underlined. *Vcp*^{A232E} allele contains the base pair changes introducing the A-to-E mutation and the *Dra* I cut site. Two additional silent mutations were added to prevent recutting by Cas9 following homology directed repair. All edited nucleotides are shown in red letters. C, DNA sequence of a heterozygous (A232E/+) mouse showing missense A-to-E mutation and other silent mutations including the *Dra* I cut site. D, a representative agarose gel shows PCR-amplified DNA bands digested with *Dra* I which distinguishes between mice homozygous for the mutant allele, *Vcp*^{A232E} (473 bp and 302 bp), WT mice homozygous for the WT allele, *Vcp*⁺ (775 bp), and heterozygous A232E/+ mice carrying one copy each of WT (775 bp) and mutant (473 and 302 bp) alleles. E, body weight changes of WT (circles) and A232E/+ (squares) mice under SD (filled symbols) or HFD (open symbols). HFD was started at the age of 8 weeks. Values are means ± SEM (n = 5–8 per group). † or *p < 0.05, **p < 0.01 as determined by 2-way ANOVA for comparing groups (E). HFD, high-fat diet; SD, standard diet; VCP, valosin-containing protein.

allele by *Dra* I produced 473-bp and 302-bp products, while the WT allele 775-bp product was not digested. Although breeding of heterozygous A232E/+ mice yielded in the generation of live mice homozygous for the *Vcp*^{A232E} mutation, they died within a few days after birth. Thus, A232E/+ mice were used for analyses in the present study.

There was no difference in appearance between WT and A232E/+ mice fed standard diet (SD) (Fig. S1). Body weight was slightly but significantly decreased in A232E/+ mice compared with WT from birth (Fig. 1E). We fed mice HFD from the age of 8 weeks. Although the mean body weight in A232E/+ mice was always lower than that in WT mice under HFD, the significant difference disappeared over time (Fig. 1E).

Phenotypic analyses of the liver and white adipose tissue in A232E/+ mice fed SD or HFD

Under SD, no macroscopic difference in abdominal contents, including the liver and epididymal white adipose tissue (eWAT) between WT and A232E/+ mice, was detected (Fig. 2A). In fact, there was no difference in liver and eWAT weights, liver histology, and liver TG content between WT and A232E/+ mice under SD (Fig. 2, B–E). HFD feeding apparently increased liver size and intra-abdominal fat mass in WT mice (Fig. 2A). However, this enlargement of the liver was ameliorated in A232E/+ mice when compared to WT mice (Fig. 2A). HFD-induced increases in liver weight and liver TG content were also attenuated in A232E/+ mice (Fig. 2, B and E). Histological examination by hematoxylin-eosin (H&E) or Oil Red

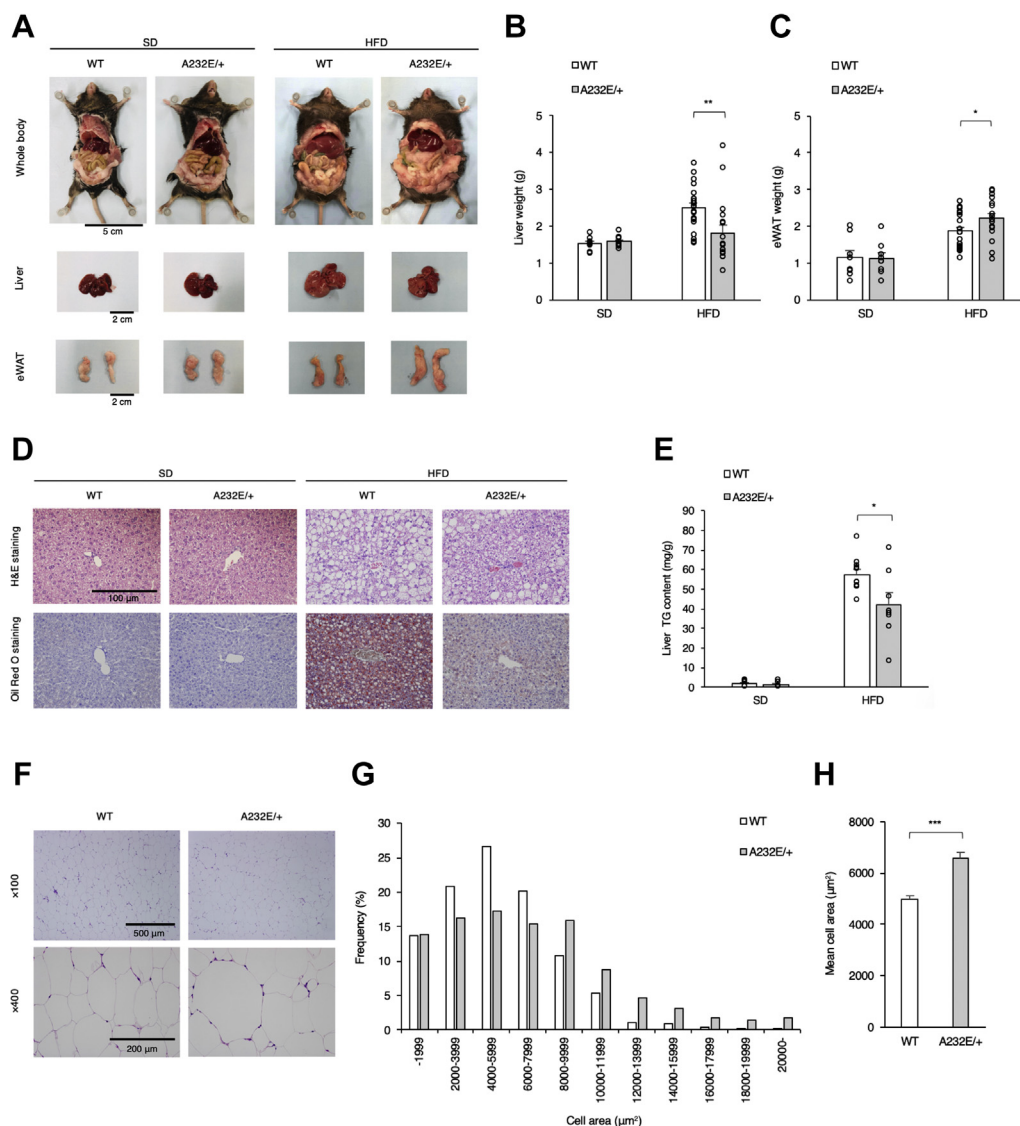


Figure 2. Phenotypes of the liver and eWAT in WT and A232E/+ mice fed SD or HFD. A, macroscopic images of the abdominal cavity (top), liver (middle), and eWAT (bottom) in 30-week-old male mice. B and C, tissue weights of the liver and eWAT in mice fed SD (B, n = 8–9 per group) or HFD (C, n = 18–22 per group). D, histological images of the liver stained with H&E (top) or Oil Red O (bottom). The original magnification is $\times 200$. E, liver TG contents (SD, n = 5–6 per group; HFD, n = 8–11 per group). F, histological images of the eWAT stained with H&E in mice fed HFD. Original magnifications are $\times 100$ (top) and $\times 400$ (bottom). G and H, adipocyte size distribution (G) and mean cross-sectional area of adipocytes (H) in the eWAT from mice fed HFD. Values are means \pm SEM. * $p < 0.05$, ** $p < 0.01$, *** $p < 0.005$ as determined by 2-tailed Student’s *t* test for comparing two groups (B, C, E and H). eWAT, epididymal white adipose tissue; HFD, high-fat diet; SD, standard diet; TG, triglyceride.

VCP and proteolytic processing of SREBP1

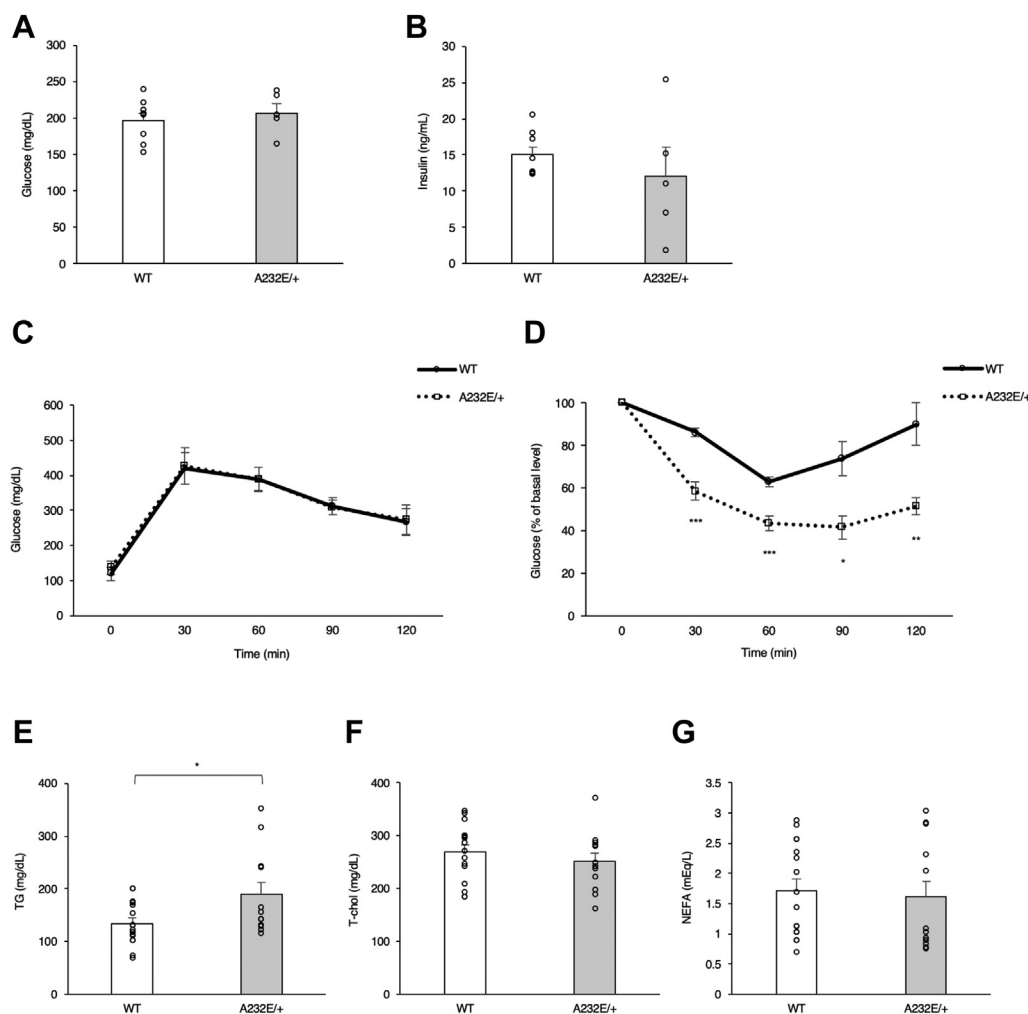


Figure 3. Glucose and lipid metabolisms in WT and A232E/+ mice fed HFD. A and B, ad libitum plasma glucose and insulin concentrations (n = 5–8 per group). C and D, plasma glucose concentrations during IPGTT and IPITT (n = 5–6 per group). E–G, ad libitum plasma TG, total cholesterol, and NEFA concentrations (n = 12–16 per group). Values are means ± SEM. * $p < 0.05$, ** $p < 0.01$, *** $p < 0.005$ as determined by 2-tailed Student's *t* test for comparing two groups. HFD, high-fat diet; IPGTT, intraperitoneal glucose tolerance test; IPITT, intraperitoneal insulin tolerance test; NEFA, nonesterified fatty acid; TG, triglyceride.

O staining showed a large number of lipid droplets of various sizes in the liver in WT mice fed HFD (Fig. 2D). Both the number and size of lipid droplets in the liver were also decreased in A232E/+ mice (Fig. 2D). In contrast, after HFD feeding, intra-abdominal fat mass of A232E/+ mice was further increased compared to WT mice (Fig. 2A). eWAT weight in A232E/+ mice was significantly heavier than that in WT mice (Fig. 2C). Microscopic examination of eWAT showed the enlargement of adipocytes in A232E/+ mice (Fig. 2F). The adipocyte size distribution deviated to the right, and the mean cross-sectional adipocyte area was significantly increased in A232E/+ mice compared to WT mice (Fig. 2, G and H). On the other hand, no significant difference in weights of tissues other than the liver and WAT was detected between A232E/+ and WT mice fed HFD (Fig. S2).

Glucose and lipid metabolisms in A232E/+ mice fed HFD

Since the liver and WAT, two major insulin target tissues, were affected, we examined glucose and lipid metabolisms in A232E/+ mice fed HFD. There was no significant difference in

both plasma glucose and insulin concentrations between WT and A232E/+ mice fed HFD (Fig. 3, A and B). Glucose tolerance examined by intraperitoneal glucose tolerance test (IPGTT) was also unchanged between WT and A232E/+ mice (Fig. 3C). However, insulin sensitivity examined by intraperitoneal insulin tolerance test (IPITT) was significantly improved in A232E/+ mice compared to WT mice (Fig. 3D). As to lipid metabolism, plasma TG concentration was slightly but significantly increased in A232E/+ mice compared to WT mice (Fig. 3E), while plasma nonesterified fatty acid (NEFA) and total cholesterol concentrations were unchanged (Fig. 3, F and G).

ATP concentration and expressions of VCP and ER stress markers in the liver in A232E/+ mice fed HFD

A232E is a gain-of-function mutation that enhances ATPase activity of VCP (11, 21). We examined whether A232E mutation causes excessive consumption of ATP and leads to a cellular lack of ATP and ER stress. There was no change of ATP concentration and expressions of ER stress markers in

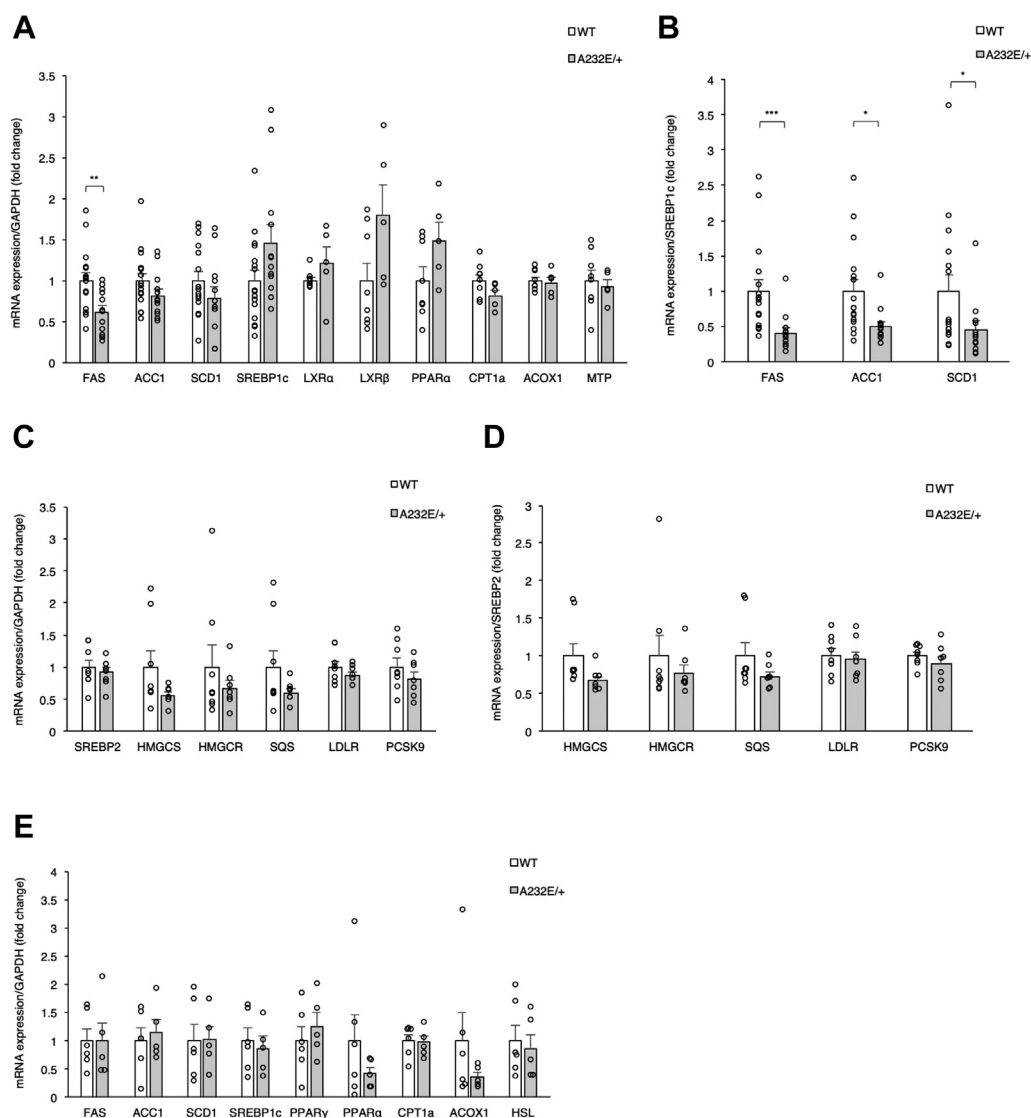


Figure 4. mRNA expressions of various genes related to TG metabolism in the liver and eWAT of WT and A232E/+ mice fed HFD. A, mRNA expressions of genes related to TG metabolism in the liver (FAS-SREBP1c, $n = 12-16$ per group; LXR α -MTP, $n = 5-8$ per group). B, relative mRNA expressions of SREBP1c target genes to SREBP1c gene in the liver ($n = 12-16$ per group). C, mRNA expressions of SREBP2 and its target genes in the liver ($n = 7-8$ per group). D, relative mRNA expressions of SREBP2 target genes to SREBP2 gene in the liver ($n = 7-8$ per group). E, mRNA expressions of genes related to TG metabolism in the eWAT ($n = 5-6$ per group). mRNA expression levels were normalized by GAPDH. The fold change is relative to WT mice. Values are means \pm SEM. * $p < 0.05$, ** $p < 0.01$, *** $p < 0.005$ as determined by 2-tailed Student's t test for comparing two groups. ACC1, acetyl-CoA carboxylase 1; FAS, fatty acid synthase; ACOX1, acyl-CoA oxidase 1; CPT1a, carnitine palmitoyltransferase 1a; eWAT, epididymal white adipose tissue; HFD, high-fat diet; HMGR, 3-hydroxy-3-methylglutaryl-CoA reductase; HMGCS, 3-hydroxy-3-methylglutaryl-CoA synthase; LDLR, low-density lipoprotein receptor; LXR α , liver X receptor α ; MTP, microsomal triglyceride transfer protein; PCSK9, proprotein convertase subtilisin/kexin type 9; PPAR α , peroxisome proliferator-activated receptor α ; SCD1, stearoyl-CoA desaturase 1; SQS, squalene synthase; SREBP1, sterol regulatory element-binding protein 1; TG, triglyceride.

the liver in at least 20-week-old A232E/+ mice compared to WT control mice under HFD feeding (Fig. S3, A–C). At this time, we also confirmed no change of VCP expressions in the liver (Fig. S3, B and C). Thus, it is unlikely that the change of ATPase activity in VCP induced by A232E mutation affected the lipid accumulation in the liver.

mRNA expressions of genes related to TG metabolism in the liver and eWAT in A232E/+ mice

To investigate the mechanism by which the heterozygous *Vcp*^{A232E} mutation ameliorated fatty liver and further increased WAT weight in mice fed HFD, we examined mRNA

expressions of genes related to TG metabolism in the liver and eWAT in A232E/+ mice fed HFD (Fig. 4). In the liver, mRNA expression of fatty acid synthase (FAS), a lipogenic gene positively regulated by SREBP1c (28), was significantly decreased in A232E/+ mice compared to WT mice (Fig. 4A). However, mRNA expressions of SREBP1c and its positive regulators, liver X receptor α and β , were statistically unchanged. Although mRNA expressions of other lipogenic genes positively regulated by SREBP1c such as acetyl-CoA carboxylase 1 and stearoyl-CoA desaturase 1 (SCD1) were statistically unchanged, relative mRNA expressions of these genes to that of SREBP1c were significantly decreased in A232E/+ mice compared to WT mice (Fig. 4B). As to genes

VCP and proteolytic processing of SREBP1

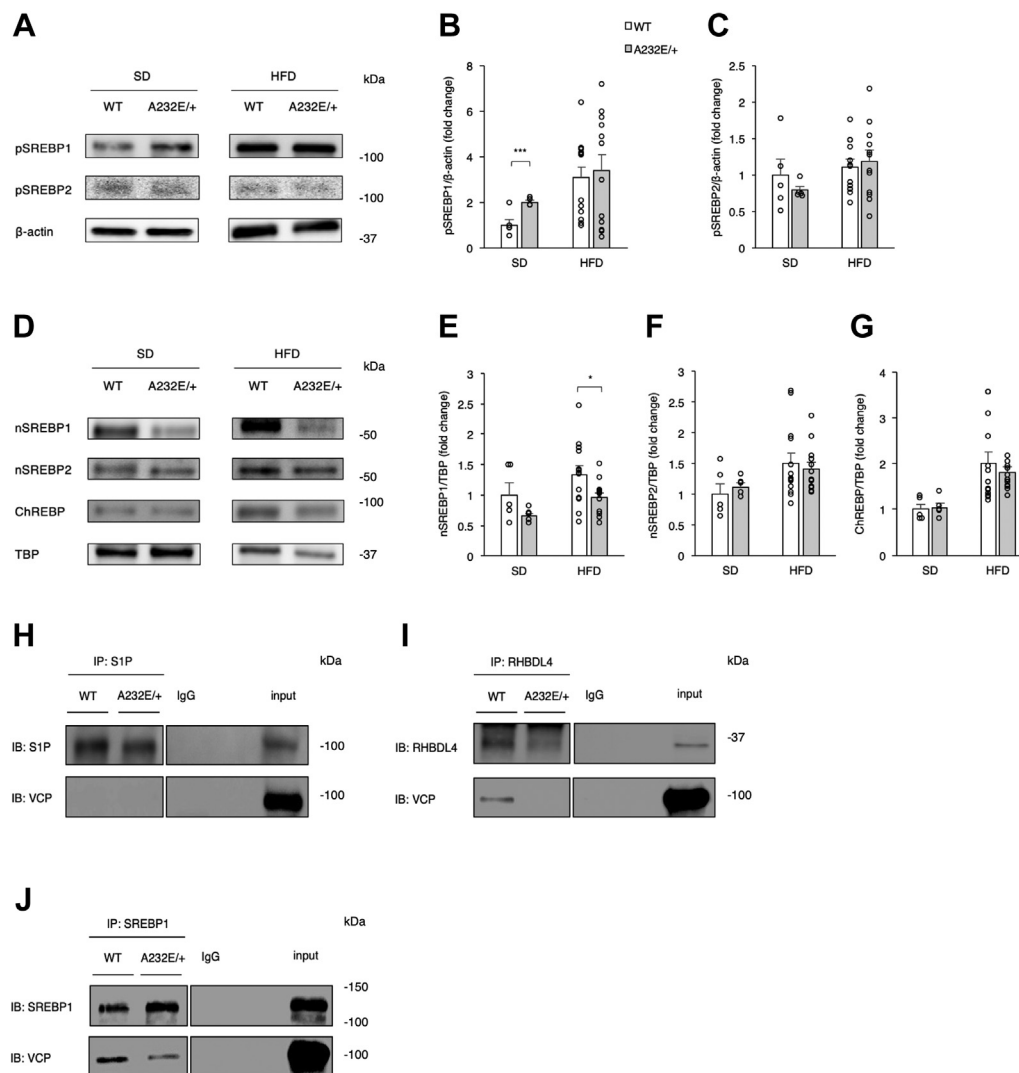


Figure 5. Protein expressions of precursor (p) and nuclear (n) forms of SREBP1 and co-immunoprecipitation assays for interactions of VCP with S1P, RHBDL4, or SREBP1 using liver lysates of WT and A232E/+ mice. *A*, representative images of Western blot analyses for pSREBP1, pSREBP2, and β -actin protein levels in the plasma membrane fraction of the liver tissue. *B* and *C*, ratio of signal intensities of pSREBP1 (*B*) and pSREBP2 (*C*) to β -actin in Western blot analyses. *D*, representative images of Western blot analyses for nSREBP1, nSREBP2, ChREBP, and TBP protein levels in the nuclear fraction of the liver tissue. *E–G*, ratio of signal intensities of nSREBP1 (*E*), nSREBP2 (*F*), and ChREBP (*G*) to TBP in Western blot analyses. *H*, immunoblots for S1P and VCP using proteins immunoprecipitated with anti-S1P antibody. *I*, immunoblots for RHBDL4 and VCP using proteins immunoprecipitated with anti-RHBDL4 antibody. *J*, immunoblots for SREBP1 and VCP using proteins immunoprecipitated with anti-SREBP1 antibody. Liver lysates of mice fed HFD were used for co-immunoprecipitation assays. Input indicates liver lysates without immunoprecipitation. IgG indicates control proteins immunoprecipitated with isotype antibody. Spliced-together lanes were run on the same gel but were noncontiguous. *B*, *C*, *E–G*, values are means \pm SEM (SD, $n = 5$ per group; HFD, $n = 12–13$ per group). Fold change is relative to WT mice fed SD. * $p < 0.05$, ** $p < 0.01$, *** $p < 0.005$ as determined by 2-tailed Student's *t* test for comparing two groups. ChREBP, carbohydrate-responsive element-binding protein; HFD, high-fat diet; SD, standard diet; S1P, site-1 protease; SREBP1, sterol regulatory element-binding protein 1; TBP, TATA box-binding protein; TG, triglyceride; VCP, valosin-containing protein.

related to β -oxidation such as peroxisome proliferator-activated receptor alpha and carnitine palmitoyltransferase 1a and acyl-CoA oxidase 1 and gene related to lipoprotein assembly and secretion such as microsomal triglyceride transfer protein, no significant difference was observed in their mRNA expressions (Fig. 4A). We next examined mRNA expressions of SREBP2 and its target genes in the liver, but none of them were significantly changed in A232E/+ mice compared to WT mice (Fig. 4C). Relative mRNA expressions of SREBP2 target genes to that of SREBP2 were also unchanged (Fig. 4D). In eWAT, there was no significant difference in mRNA expressions of genes related to lipogenesis, fatty acid β -oxidation, and lipolysis between A232E/+ and WT mice (Fig. 4E). These

results indicate that the amelioration of fatty liver in A232E/+ mice is due to the downregulation of lipogenic gene expressions in the liver, which is contrary to that of SREBP1c.

Protein expressions of precursor and nuclear forms of SREBP1 in the liver of A232E/+ mice fed SD or HFD

SREBP1 is a membrane-bound transcription factor that can activate the expressions of its target genes upon proteolytic processing (9). Namely, proteolytic cleavage of precursor (p) form of SREBP1 releases nuclear (n) form of SREBP1 into the cytoplasm. Then, nSREBP1 migrates to the nucleus and activates the promoters of the target genes. Thus, we investigated

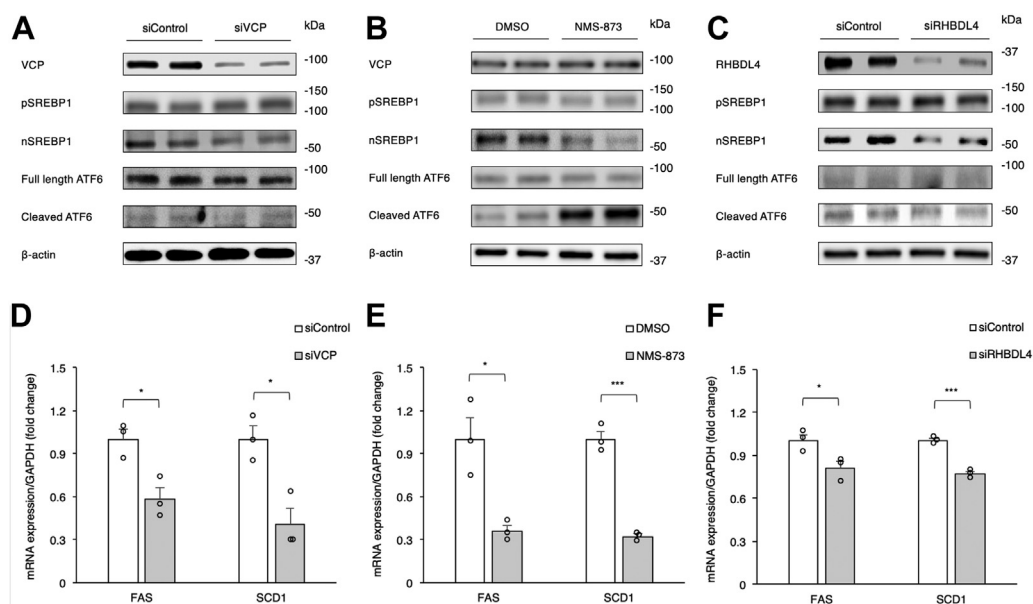


Figure 6. Knockdown experiments of VCP or RHBDL4 with siRNA and inhibition experiment of VCP with an allosteric inhibitor in HepG2 cells. A–C, Western blot analyses for VCP, pSREBP1, nSREBP1, full-length ATF6, cleaved ATF6, and β -actin protein levels in HepG2 cells with or without VCP siRNA (A), NMS-873, an allosteric VCP inhibitor, (B) or RHBDL4 siRNA (C). D–F, mRNA expressions of FAS and SCD1 in HepG2 cells with or without VCP siRNA (D), NMS-873 (E), or RHBDL4 siRNA (F) ($n = 3$). mRNA expression levels were normalized by GAPDH. The fold change is relative to HepG2 cells transfected with control siRNA (D and F) or HepG2 cells treated with DMSO (E). Values are means \pm SEM. * $p < 0.05$, ** $p < 0.01$, *** $p < 0.005$ as determined by 2-tailed Student's t test for comparing two groups. ATF6, activating transcription factor 6; FAS, fatty acid synthase; SCD1, stearyl-CoA desaturase 1; SREBP1, sterol regulatory element-binding protein 1; VCP, valosin-containing protein.

the protein expressions of pSREBP1 and nSREBP1 in the liver separately. The protein expression of pSREBP1 in the plasma membrane fraction was significantly increased in A232E/+ mice compared to WT mice under SD and tended to be increased under HFD (Fig. 5, A and B). In contrast, the protein expression of nSREBP1 in the nuclear fraction tended to be decreased under SD and was significantly decreased under HFD in A232E/+ mice compared to WT mice (Fig. 5, D and E). These results indicate that the proteolytic processing of SREBP1 is impaired in A232E/+ mice. We also investigated protein expressions of pSREBP2 and nSREBP2 in the liver, but both of them were not significantly altered in A232E/+ mice compared to WT mice (Fig. 5, A, C, D and F). Protein expression of carbohydrate-responsive element-binding protein, another important transcription factor that positively regulates lipogenic genes (9), was not decreased in A232E/+ mice irrespective of diet (Fig. 5, D and G).

Interactions of VCP with S1P, RHBDL4, or SREBP1 in the liver of A232E/+ mice fed HFD

SCAP, S1P, and S2P participate in the proteolytic processing of SREBPs (9). However, co-immunoprecipitation assay showed no binding of S1P to VCP in the liver of both WT and A232E/+ mice (Fig. 5H). In fission yeast, Rbd2, a rhomboid protease, is necessary for proteolytic processing of SREBP (22). This Rbd2 binds to cdc48, the yeast homolog of VCP, and inhibition of the binding between them impairs the proteolytic processing of SREBP (23). In mammals, RHBDL4, a mammalian homolog of rhomboid protease, binds to VCP at

the site of ER-associated degradation (25). In addition, it was recently reported that RHBDL4 directly cleaves SREBP1 (29). Thus, we next examined the interactions among VCP, SREBP1, and RHBDL4 in the liver. Co-immunoprecipitation assay showed binding between VCP and RHBDL4 in WT mice, but not in A232E/+ mice (Fig. 5J). In addition, binding between VCP and SREBP1 was detected in WT mice and was attenuated in A232E/+ mice (Fig. 5J). These results indicate that the A232E mutation disrupts the ability of VCP to interact with RHBDL4 and SREBP1.

Effect of knockdown of VCP or RHBDL4 or inhibition of VCP on the processing of SREBP1 in HepG2 cells

To investigate the roles of VCP and RHBDL4 in the proteolytic cleavage of SREBP1 in mammalian hepatocytes, we performed siRNA knockdown experiments of VCP and RHBDL4 and inhibition experiment of VCP by an allosteric inhibitor in HepG2 cells. VCP siRNA effectively decreased the protein expression of VCP in HepG2 cells (Fig. 6A). At this time, nSREBP1 protein level was apparently decreased while pSREBP1 protein level was unchanged (Fig. 6A). NMS-873, an allosteric VCP inhibitor, did not affect the protein expressions of VCP and pSREBP1 but decreased nSREBP1 protein level in HepG2 cells (Fig. 6B). RHBDL4 siRNA also effectively decreased the protein levels of RHBDL4 and nSREBP1, while pSREBP1 protein level was unchanged in HepG2 cells (Fig. 6C). These results indicate that both VCP and RHBDL4 are involved in the proteolytic processing of SREBP1 in hepatocytes. Activating transcription factor 6

VCP and proteolytic processing of SREBP1

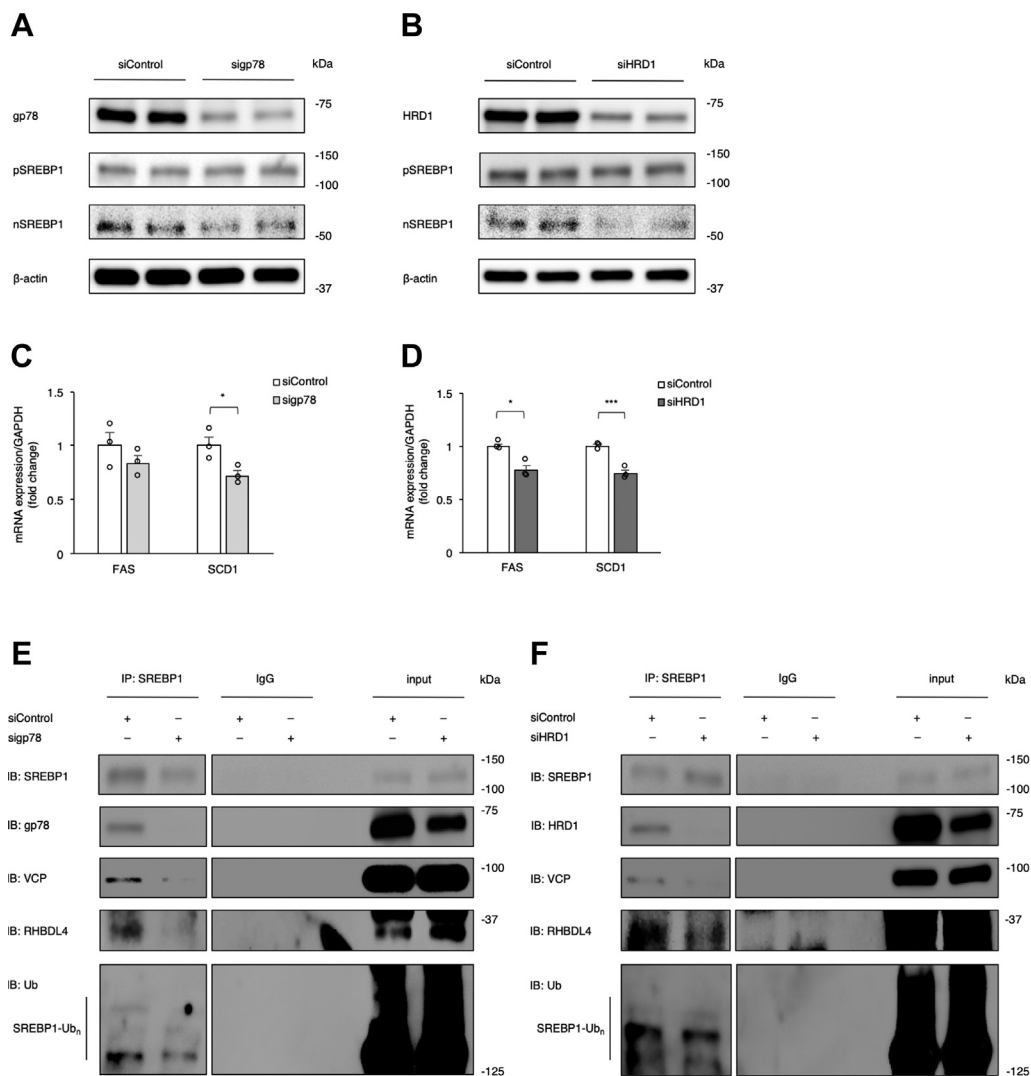


Figure 7. Knockdown experiments of E3 ligase, gp78, or HRD1 with siRNA in HepG2 cells. *A* and *B*, Western blot analyses for gp78, pSREBP1, nSREBP1, and β -actin protein levels with or without gp78 siRNA (*A*) and for HRD1, pSREBP1, nSREBP1, and β -actin protein levels with or without HRD1 siRNA (*B*). *C* and *D*, mRNA expressions of FAS and SCD1 with or without gp78 siRNA (*C*) and with or without HRD1 siRNA (*D*) ($n = 3$). mRNA expression levels were normalized by GAPDH. The fold change is relative to HepG2 cells transfected with control siRNA. *E* and *F*, Western blot analyses for SREBP1, gp78, VCP, RHBDL4, and ubiquitin using proteins immunoprecipitated with anti-SREBP1 antibody with or without gp78 siRNA (*E*) and for SREBP1, HRD1, VCP, RHBDL4, and ubiquitin using proteins immunoprecipitated with anti-SREBP1 antibody with or without HRD1 siRNA (*F*). Input indicates cell lysates without immunoprecipitation. IgG indicates control proteins immunoprecipitated with isotype antibody. Spliced-together lanes were run on the same gel but were noncontiguous. *C* and *D*, values are means \pm SEM. * $p < 0.05$, ** $p < 0.01$, *** $p < 0.005$ as determined by 2-tailed Student's *t* test for comparing two groups. FAS, fatty acid synthase; HRD1, HMG-CoA reductase degradation protein 1; SCD1, stearyl-CoA desaturase 1; SREBP1, sterol regulatory element-binding protein 1; VCP, valosin-containing protein.

(ATF6), an ER stress-regulated transmembrane transcription factor, is known to be cleaved by S1P and S2P as well as SREBP1 (30). Consistent with the result indicating no binding of VCP with S1P (Fig. 5H), neither knockdown nor inhibition of VCP reduced the level of cleaved ATF6 protein (Fig. 6, A and B). In addition, the knockdown of RHBDL4 did not affect the cleaved ATF6 protein level, indicating that RHBDL4 is not participated in the proteolytic processing of ATF6 (Fig. 6C).

We also examined the effect of knockdown of VCP or RHBDL4, or inhibition of VCP on mRNA expressions of SREBP1 target genes, including FAS and SCD1, in HepG2 cells. All these procedures significantly decreased mRNA expressions of both FAS and SCD1, consistent with the

reduction of nSREBP1, the transcriptionally active form of SREBP1 (Fig. 6, D–F).

Effect of knockdown of gp78 or HMG-CoA reductase degradation protein 1 on the processing of SREBP1 in HepG2 cells

In yeast, it has been demonstrated that Dsc E3 ubiquitin ligase ubiquitinylates SREBP prior to cleavage by Rbd2, suggesting that Cdc48 recognizes and recruits ubiquitinylated SREBP to Rbd2 (23). On the other hand, it has been reported that liver-specific knockout of glycoprotein 78 (gp78) or HMG-CoA reductase degradation protein 1 (HRD1), both of which are E3 ligase and resemble Dsc E3 ligase in their subunits and organization, ameliorates fatty liver in mice (31–33).

Co-immunoprecipitation assays showed that both of gp78 and HRD1 bound to SREBP1 in mouse liver in spite of the presence or absence of A232E mutation (Fig. S4). Thus, we next performed knockdown experiments of gp78 and HRD1 with siRNA in HepG2 cells to investigate the roles of gp78 and HRD1 in the proteolytic cleavage of SREBP1 in mammalian hepatocytes. gp78 siRNA effectively decreased protein expression of gp78 in HepG2 cells (Fig. 7A). At this time, nSREBP1 protein level was decreased while pSREBP1 protein level was unchanged (Fig. 7A). HRD1 siRNA also effectively decreased protein levels of HRD1 and nSREBP1, while pSREBP1 protein level was unchanged (Fig. 7B). We also examined the effect of knockdown of gp78 or HRD1 on mRNA expressions of SREBP1 target genes in HepG2 cells. Each knockdown significantly decreased mRNA expressions of FAS and SCD1, consistent with the reduction of nSREBP1 (Fig. 7, C and D). Lastly, we examined the effect of knockdown of gp78 or HRD1 on the interactions between VCP and SREBP1 and between RHBDL4 and SREBP1 in HepG2 cells. Co-immunoprecipitation assays showed that both interactions between VCP and SREBP1 and between RHBDL4 and SREBP1 detected in control cells were attenuated by knockdown of gp78 and HRD1, respectively (Fig. 7, E and F). At this time, ubiquitinated SREBP1 level was also attenuated by knockdown of gp78 and HRD1, respectively (Fig. 7, E and F). These results suggest that VCP recognizes SREBP1 ubiquitinated by E3 ligases such as gp78 and HRD1 and recruits it to RHBDL4 for its proteolytic activation in mammals.

Discussion

In the present study, we investigated the pathophysiological role of VCP in the lipid accumulation in the liver to clarify the mechanism underlying the amelioration of HFD-induced fatty liver in A232E/+ mice. We examined mRNA expressions of genes related to lipid metabolism in the liver and found that those of SREBP1 target genes such as FAS, acetyl-CoA carboxylase 1, and SCD1 were decreased relatively to that of SREBP1c, suggesting the impairment of translation or post-translational modification of SREBP1c (Fig. 4). SREBP1 is synthesized as a membrane protein located in the ER (9). Following cleavage, the mature protein translocates to the nucleus and activates the transcription of lipogenic genes (9). In the liver of A232E/+ mice, although full-length SREBP1 in the membrane fraction was not decreased, mature SREBP1 in the nuclear extract was obviously decreased (Fig. 5). These results indicate that A232E mutation in VCP impairs the proteolytic processing of SREBP1. While HFD-induced fatty liver was ameliorated in A232E/+ mice compared to WT mice, there was no significant difference in liver TG content between them under SD feeding (Fig. 2). This might be due to the increased role of SREBP1 in accordance with the increased TG synthesis in the liver by HFD feeding.

Some previous reports suggest the role of VCP in the activation of SREBP1. Rbd2, a yeast homolog of rhomboid proteases, is required for the activation of SREBP in yeast (22).

Cdc48, the yeast homolog of VCP, binds to Rbd2, and inhibition of this binding impairs SREBP processing in yeast (23, 24). Moreover, it was demonstrated that RHBDL4, one of mammalian rhomboid proteases, interacts with VCP during ERAD (25). Recently, it was reported that RHBDL4 directly cleaves SREBP1 independently of the SCAP-INSIG system in mammalian cells (29). In the present study, using co-immunoprecipitation technique, we observed interactions of VCP with RHBDL4 and SREBP1 in the liver of WT mice and these interactions were attenuated in A232E/+ mice (Fig. 5, I and J). Because the activation of SREBP1 was impaired in A232E/+ mice in which the interaction of VCP with RHBDL4 was attenuated, the interaction of VCP with RHBDL4 might be required for the proteolytic cleavage of SREBP1 by RHBDL4 in mammals. Results of the knockdown experiment using VCP siRNA and VCP inhibition experiment with an allosteric inhibitor in a human hepatocyte cell line support this idea. Both knockdown and inhibition of VCP impaired the proteolytic processing of SREBP1 (Fig. 6, A and B).

In yeast, Dsc E3 ubiquitin ligase acts on SREBP prior to the cleavage by Rbd2 (23). Cdc48 acts to recruit ubiquitinated substrates (23). Thus, it has been suggested that Cdc48 recognizes SREBP ubiquitinated by Dsc E3 ligase and recruits it to Rbd2 for its proteolytic activation in yeast (23). Dsc E3 ligase is a complex composed of five subunits, and its architecture resembles those of gp78 and HRD1, mammalian E3 ligases. Thus, we investigated the roles of gp78 and HRD1 in the proteolytic activation of SREBP1 in a human hepatocyte cell line. Knockdown experiments using siRNA and co-immunoprecipitation analyses demonstrated that knockdown of gp78 or HRD1 suppressed the activation of SREBP1 and the interactions between VCP and SREBP1 and between RHBDL4 and SREBP1 (Fig. 7). These results indicate that the ubiquitination of SREBP1 by E3 ligases such as gp78 and HRD1 might be required for the recognition of SREBP1 by VCP in mammals. Collectively, it is suggested that VCP recognizes SREBP1 ubiquitinated by E3 ligases and recruits it to RHBDL4 for its proteolytic activation in mammals.

The fact that A232E mutation impairs the bindings of VCP to RHBDL4 and SREBP1 indicates that the alanine residue at position 232 in the amino acid sequence of VCP is important not only for ATPase activity but also for the binding to RHBDL4 and SREBP1. VCP has been shown to recognize ubiquitinated protein through Npl4/Ufd1 heterodimer, a major ubiquitin-recruiting cofactor (34). Thus, it is thought that VCP also binds to ubiquitinated SREBP1 through Npl4/Ufd1 heterodimer. Many VCP cofactors including RHBDL4 and Npl4/Ufd1 heterodimer have been shown to bind to the N-terminal domain of VCP (13). The conformation of the N-terminal domain is regulated by the D1 domain (35). Human pathogenic mutations including A232E which occurs in the D1 domain have been shown to alter the conformation of the N-terminal domain and affect its cofactor association (36). Thus, it is possible that A232E mutation alters the binding affinity of the N-terminal domain to both RHBDL4 and Npl4/Ufd1.

VCP and proteolytic processing of SREBP1

While HFD-induced fatty liver was ameliorated, adipose tissue weight was significantly increased in A232E/+ mice compared to WT mice (Fig. 2). Although A232E/+ mouse is a global knock-in one, it is unlikely that A232E mutation in VCP expressed in adipose tissue directly affected the adipose phenotype since mRNA expressions of genes related to lipid metabolism including lipogenesis in the adipose tissue were unchanged in A232E/+ mice. In cases of liver-specific transgenic mice, fatty liver resistant models show the increase of fatty acid synthesis in adipose tissue (31, 37). These results suggest that the increase in adipose tissue weight in A232E/+ mice is a secondary effect of the amelioration of fatty liver.

It has been reported that RHBDL4 interacts with VCP during ERAD (25). The present study demonstrates that A232E mutation disrupts the interaction between VCP and RHBDL4. Although we analyzed the effect of A232E mutation on the lipid accumulation in the liver, phenotypes associated with ERAD in A232E/+ mice have not yet been investigated. There was no visible difference between A232E/+ and WT mice at least at the age of up to 20 weeks other than the amelioration of fatty liver and the increase of adipose tissue weight. A certain aging may be necessary for the development of ERAD-associated phenotypes.

In conclusion, the present study revealed the role of VCP in lipid accumulation in the liver. VCP engages in the proteolytic processing of SREBP1 through its interaction with RHBDL4, that is to say, VCP may act as a substrate adapter for RHBDL4. A232E mutation impairs the proteolytic processing of SREBP1 by RHBDL4 through disrupting the interaction between VCP and RHBDL4 and attenuates fatty liver. New treatment targeting VCP or RHBDL4 is expected to be developed in the future.

Experimental procedures

Animals

Mice were housed under controlled conditions of temperature ($23\text{ }^{\circ}\text{C} \pm 1\text{ }^{\circ}\text{C}$), humidity ($55\% \pm 5\%$), and lighting (light phase: 7:30–19:30) and fed ad libitum SD (MF; Oriental Yeast). For HFD loading, mice were fed an ad libitum HFD containing 20% kcal for kcal (kcal/kcal) protein, 20% kcal/kcal carbohydrate, and 60% kcal/kcal fat (D12492; Research Diets) from the ages of 8 weeks. Twenty-week-old male mice were used for analysis unless otherwise described. All animal experiments were carried out after receiving approval from the Institutional Animal Experiment Committee and in accordance with the Institutional Regulation for Animal Experiments at Jichi Medical University. *Vcp*^{A232E/+}-mutant mice (referred to as A232E/+ mice) were generated by CRISPR/Cas9 and maintained on C57BL/6J background. Details of the targeting of *Vcp* are provided in the following sections.

Generation of A232E/+ mice

CRISPR/Cas9 constructs and reagents were designed to introduce the human single-base-pair missense mutation

resulting in the A232E substitution within exon six of *Vcp* (Fig. 1A) by CRISPR/Cas9 in combination with a single-stranded oligodeoxynucleotide (ssODN) for use in homology-dependent repair (HDR). The murine and human VCP proteins are 100% identical at the amino acid level (27). A gRNA was selected to direct Cas9-mediated cutting near the target nucleotide. The ssODN contained the desired sequence to introduce the A232E amino acid change, a silent base change to reduce the likelihood of recutting of the desired allele, and a silent base change to generate a *Dra* I site for screening (5'-AGATAAAGGAGATGGTGGAGCTGCCACTGAGACAT CCTGCACTGTTTAAAGAGATTGGTGTAAAGGTGAGTATCCTAAGGTCTGTGGGGAGTCT-3') (Fig. 1B). Embryos were collected 0.5 days after fertilization. A ribonucleoprotein complex of gRNA and Cas9 protein were co-microinjected with the ssODN donor into embryo pronuclei. Embryos were surgically implanted into the oviducts of 0.5-day pseudopregnant females. After screening of offspring, a single male with the desired modifications was used to establish a line of A232E/+ mice on a C57BL/6J background. Genotypes of subsequent mice were confirmed by PCR amplification of restriction enzyme digests and Sanger sequencing (Fig. 1, C and D).

Liver histology

Livers were sampled from 20-week-old mice, fixed in 10% neutrally buffered formalin, and embedded in paraffin. Histological sections of 5-mm thickness were stained with hematoxylin and eosin or Oil Red O and examined by light microscopy.

Adipose tissue histology and adipocyte size measurement

eWAT were sampled from 20-week-old mice, fixed in 10% neutrally buffered formalin, and embedded in paraffin. Histological sections of 5-mm thickness were stained with hematoxylin and eosin and examined by light microscopy. Adipocyte size was evaluated in a mouse from each group and two random fields (magnification $\times 100$) per mouse. To measure cross-sectional adipocyte area, micrographs were taken with a microscope (DP70; Olympus) and analyzed with ImageJ software (National Institutes of Health).

Biochemical assays

Blood was obtained from the retro-orbital sinus under ad libitum feeding unless otherwise mentioned. Plasma glucose concentration was measured using a glucose assay kit (Wako Pure Chemical Industries). Plasma insulin concentration was measured using an insulin-ELISA kit (Morinaga Institute of Biological Science). Plasma TG, NEFA, and total cholesterol concentrations were measured using enzymatic kits (Triglyceride E-test Wako, NEFA C-test Wako, and Cholesterol E-test Wako, respectively; Wako Pure Chemical Industries). To measure liver TG content, we sampled livers from 20-week-old mice and immediately froze them in liquid nitrogen. Lipids were extracted with isopropyl alcohol heptane (1:1 volume for volume). After evaporation of the solvent, we resuspended lipids in 99.5% volume for volume ethanol, and

TG content was measured by an enzymatic kit (Triglyceride E-test Wako).

Glucose and insulin tolerance tests

IPGTT and IPITT were performed after overnight fasting in 20-week-old mice. For the IPGTT, mice received 1.0 g/kg glucose, and blood was sampled from the tail vein before and 30, 60, 90, and 120 min after the glucose load. For the IPITT, mice received 0.5 IU/kg insulin (Novolin R; Novo Nordisk Japan) by intraperitoneal injection. Blood was sampled from the tail vein before and 30, 60, 90, and 120 min after the insulin load.

Real-time quantitative RT-PCR

After sampling, tissues were immediately frozen in liquid nitrogen and stored at -80°C until use for RNA isolation. RNA of livers and cultured cells was prepared using Trizol (Thermo Fisher Scientific) reagent, and RNA of epididymal WAT was prepared using RNeasy Lipid Tissue Mini Kit (Qiagen) following the manufacturer's protocol. The Quality and the concentrations of the extracted RNA were checked using the Nano-Drop 2000 (Thermo Fisher Scientific). Single-stranded cDNA was synthesized from 1 μg of total RNA using iScript cDNA Synthesis Kit (Bio-Rad Laboratories) for RT-PCR, according to the manufacturer's instructions. All quantitative real-time PCR analyses were performed with TaqMan (Applied Biosystems) by QuantStudio 3 real-time PCR system (Applied Biosystems). mRNA expression levels were normalized to that of glyceraldehyde 3-phosphate dehydrogenase (GAPDH). The sequences of primers and probes used in the present study are shown in Table S1.

Cell culture, cell treatment, and siRNA transfection

HepG2 cells were cultured at 37°C with 5% CO_2 in DMEM medium containing 10% fetal bovine serum and 50,000 units of antibiotics (penicillin and streptomycin). For VCP inhibition experiments, cells were treated with 15 μM NMS-873 (Med-Chem Express) or treated with vehicle. For knockdown experiments, VCP siRNA (s14765; Life Technologies), RHBDL4 siRNA (s38699; Life Technologies), gp78 siRNA (s1324; Life Technologies), HRD1 siRNA (s39019; Life Technologies), or negative control siRNA (sc-37007; Santa Cruz Biotechnology) was transfected at the final concentration of 100 nM using Opti-MEM (Gibco) and Lipofectamine RNAiMAX (Invitrogen). After 48 h of treatment or transfection, cells were harvested for Western blot analysis or quantitative real-time PCR analysis.

Western blot analysis

Livers were homogenized and lysed in a solution containing 20 mM Tris (pH 7.5) 150 mM NaCl, 1 mM EDTA, 1 mM EGTA, 1% Triton X-100, 2.5 mM sodium pyrophosphate, and 1 mM sodium orthovanadate. Subcellular fractions were obtained using Subcellular Protein Fractionation Kit for Tissues (Thermo Fisher Scientific). Immunoprecipitation was performed with each antibody using Capturem IP & Co-IP kit

(Takara). Samples were separated by SDS-PAGE using 4 to 12% Bis-Tris gel (Bio-Rad) and transferred to a polyvinylidene difluoride membrane (Bio-Rad). Membranes were immunoblotted with each antibody. Amersham ECL prime (GE Healthcare Life Sciences) and ImageQuant LAS 4000mini (GE Healthcare Life Sciences) were used for the detection and quantification. Antibodies used in the present study are as follows: SREBP1 (ab3259; Abcam), VCP (ab11433; Abcam), S1P (ab140592; Abcam), SREBP2 (ab30682; Abcam), CHOP (2895; Cell Signaling Technology), BiP (3177; Cell Signaling Technology), β -actin (3700; Cell Signaling Technology), RHBDL4 (20869-1-AP; Proteintech), TBP (22006-1-AP; Proteintech), gp78 (16675-1-AP; Proteintech), HRD1 (13473-1-AP; Proteintech), Ubiquitin (10201-2-AP; Proteintech), carbohydrate-responsive element-binding protein (NB400-135; Novus Biologicals), ATF6 (NB1-40256; Novus Biologicals), and normal mouse IgG (sc-2025; Santa Cruz Biotechnology).

Statistics

Data are expressed as means \pm SEM. Comparison between or among groups was assessed by Student *t* test or 2-way ANOVA. $p < 0.05$ was considered statistically significant.

Data availability

The data supporting this study are available from the corresponding author (kebihara@jichi.ac.jp) upon reasonable request.

Supporting information—This article contains supporting information.

Acknowledgments—We thank Hitoshi Shimano, Takashi Matsuzaka, Yoshimi Nakagawa, and Song-lee Han for discussion.

Author contributions—K. S. and K. E. conceptualization; K. S. and K. E. project administration; K. S. data curation; K. S. formal analysis; K. S. investigation and writing; K. E. writing; C. E., N. S., M. I., D. Y., M. T., and S. N. investigation; S.I. resources and supervision.

Funding and additional information—This work was supported by research grants from the Japanese Ministry of Education, Culture, Sports, Science and Technology and the Japanese Ministry of Health, Labor and Welfare.

Conflict of interest—The authors declare that they have no conflicts of interest with the contents of this article.

Abbreviations—The abbreviations used are: ATF6, activating transcription factor 6; Dsc, defective for SREBP cleavage; ER, endoplasmic reticulum; ERAD, ER-associated degradation; eWAT, epididymal white adipose tissue; FAS, fatty acid synthase; gp78, glycoprotein 78; HFD, high-fat diet; HRD1, HMG-CoA reductase degradation protein 1; IPGTT, intraperitoneal glucose tolerance test; INSIG, insulin-induced gene; IPITT, intraperitoneal insulin tolerance test; NAFLD, nonalcoholic fatty liver disease; NEFA, nonesterified fatty acid; S1P, site-1 protease; S2P, site-2 protease; SCAP, SREBP cleavage-activating protein; SCD1, stearoyl-CoA desaturase I; SD, standard diet; SREBP1, sterol regulatory element-

VCP and proteolytic processing of SREBP1

binding protein 1; TG, triglyceride; VCP, valosin-containing protein.

References

1. Yoshino, S., Iwasaki, Y., Matsumoto, S., Satoh, T., Ozawa, A., Yamada, E., Kakizaki, S., Trejo, J. A. O., Uchiyama, Y., Yamada, M., and Mori, M. (2020) Administration of small-molecule guanabenz acetate attenuates fatty liver and hyperglycemia associated with obesity. *Sci. Rep.* **10**, 13671
2. Pennisi, G., Celsa, C., Spatola, F., Dallio, M., Federico, A., and Petta, S. (2019) Pharmacological therapy of non-alcoholic fatty liver disease: What drugs are available now and future perspectives. *Int. J. Environ. Res. Public Health* **16**, 4334
3. Marjot, T., Moolla, A., Cobbold, J. F., Hodson, L., and Tomlinson, J. W. (2020) Nonalcoholic fatty liver disease in adults: Current concepts in etiology, outcomes, and management. *Endocr. Rev.* **41**, 66–117
4. Younossi, Z., Anstee, Q. M., Marietti, M., Hardy, T., Henry, L., Eslam, M., George, J., and Bugianesi, E. (2018) Global burden of NAFLD and NASH: Trends, predictions, risk factors and prevention. *Nat. Rev. Gastroenterol. Hepatol.* **15**, 11–20
5. Hodson, L. (2019) Hepatic fatty acid synthesis and partitioning: The effect of metabolic and nutritional state. *Proc. Nutr. Soc.* **78**, 126–134
6. Peng, J., Yu, J., Xu, H., Kang, C., Shaul, P. W., Guan, Y., Zhang, X., and Su, W. (2018) Enhanced liver regeneration after partial hepatectomy in sterol regulatory element-binding protein (SREBP)-1c-Null mice is associated with increased hepatocellular cholesterol availability. *Cell Physiol. Biochem.* **47**, 784–799
7. Takeuchi, Y., Yahagi, N., Izumida, Y., Nishi, M., Kubota, M., Teraoka, Y., Yamamoto, T., Matsuzaka, T., Nakagawa, Y., Sekiya, M., Iizuka, Y., Ohashi, K., Osuga, J., Gotoda, T., Ishibashi, S., et al. (2010) Polyunsaturated fatty acids selectively suppress sterol regulatory element-binding protein-1 through proteolytic processing and autolysis regulatory circuit. *J. Biol. Chem.* **285**, 11681–11691
8. Monnerie, H., Romer, M., Jensen, B. K., Millar, J. S., Jordan-Sciutto, K. L., Kim, S. F., and Grinspan, J. B. (2017) Reduced sterol regulatory element-binding protein (SREBP) processing through site-1 protease (S1P) inhibition alters oligodendrocyte differentiation *in vitro*. *J. Neurochem.* **140**, 53–67
9. Xu, X., So, J. S., Park, J. G., and Lee, A. H. (2013) Transcriptional control of hepatic lipid metabolism by SREBP and ChREBP. *Semin. Liver Dis.* **33**, 301–311
10. Matthews, K. A., Ozdemir, C., and Rawson, R. B. (2010) Activation of sterol regulatory element binding proteins in the absence of Scap in *Drosophila melanogaster*. *Genetics* **185**, 189–198
11. Manno, A., Noguchi, M., Fukushi, J., Motohashi, Y., and Kakizuka, A. (2010) Enhanced ATPase activities as a primary defect of mutant valosin-containing proteins that cause inclusion body myopathy associated with Paget disease of bone and frontotemporal dementia. *Genes Cells* **15**, 911–922
12. Ide, Y., Horie, T., Saito, N., Watanabe, S., Otani, C., Miyasaka, Y., Kuwabara, Y., Nishino, T., Nakao, T., Nishiga, M., Nishi, H., Nakashima, Y., Nakazeki, F., Koyama, S., Kimura, M., et al. (2019) Cardioprotective effects of VCP modulator KUS121 in murine and porcine models of myocardial infarction. *JACC Basic Transl. Sci.* **4**, 701–714
13. Ye, Y., Tang, W. K., Zhang, T., and Xia, D. (2017) A mighty "protein extractor" of the cell: Structure and function of the p97/CDC48 ATPase. *Front. Mol. Biosci.* **4**, 39
14. Ikeda, H. O., Sasaoka, N., Koike, M., Nakano, N., Muraoka, Y., Toda, Y., Fuchigami, T., Shudo, T., Iwata, A., Hori, S., Yoshimura, N., and Kakizuka, A. (2014) Novel VCP modulators mitigate major pathologies of rd10, a mouse model of retinitis pigmentosa. *Sci. Rep.* **4**, 5970
15. Nakano, N., Ikeda, H. O., Hasegawa, T., Muraoka, Y., Iwai, S., Tsuruyama, T., Nakano, M., Fuchigami, T., Shudo, T., Kakizuka, A., and Yoshimura, N. (2016) Neuroprotective effects of VCP modulators in mouse models of glaucoma. *Heliyon* **2**, e00096
16. Nakano, M., Imamura, H., Sasaoka, N., Yamamoto, M., Uemura, N., Shudo, T., Fuchigami, T., Takahashi, R., and Kakizuka, A. (2017) ATP maintenance *via* two types of ATP regulators mitigates pathological phenotypes in mouse models of Parkinson's disease. *EBioMedicine* **22**, 225–241
17. Wang, J., Takeuchi, T., Tanaka, S., Kubo, S. K., Kayo, T., Lu, D., Takata, K., Koizumi, A., and Izumi, T. (1999) A mutation in the insulin 2 gene induces diabetes with severe pancreatic beta-cell dysfunction in the Mody mouse. *J. Clin. Invest.* **103**, 27–37
18. Harding, H. P., Zeng, H., Zhang, Y., Jungries, R., Chung, P., Plesken, H., Sabatini, D. D., and Ron, D. (2001) Diabetes mellitus and exocrine pancreatic dysfunction in perk^{-/-} mice reveals a role for translational control in secretory cell survival. *Mol. Cell* **7**, 1153–1163
19. Ozcan, L., Ergin, A. S., Lu, A., Chung, J., Sarkar, S., Nie, D., Myers, M. G., and Ozcan, U. (2009) Endoplasmic reticulum stress plays a central role in development of leptin resistance. *Cell Metab.* **9**, 35–51
20. Hosoi, T., Sasaki, M., Miyahara, T., Hashimoto, C., Matsuo, S., Yoshii, M., and Ozawa, K. (2008) Endoplasmic reticulum stress induces leptin resistance. *Mol. Pharmacol.* **74**, 1610–1619
21. Niwa, H., Ewens, C. A., Tsang, C., Yeung, H. O., Zhang, X., and Freemont, P. S. (2012) The role of the N-domain in the ATPase activity of the mammalian AAA ATPase p97/VCP. *J. Biol. Chem.* **287**, 8561–8570
22. Kim, J., Ha, H. J., Kim, S., Choi, A. R., Lee, S. J., Hoe, K. L., and Kim, D. U. (2015) Identification of Rbd2 as a candidate protease for sterol regulatory element binding protein (SREBP) cleavage in fission yeast. *Biochem. Biophys. Res. Commun.* **468**, 606–610
23. Hwang, J., Ribbens, D., Raychaudhuri, S., Cairns, L., Gu, H., Frost, A., Urban, S., and Espenshade, P. J. (2016) A Golgi rhomboid protease Rbd2 recruits Cdc48 to cleave yeast SREBP. *EMBO J.* **35**, 2332–2349
24. Burr, R., Ribbens, D., Raychaudhuri, S., Stewart, E. V., Ho, J., and Espenshade, P. J. (2017) Dsc E3 ligase localization to the Golgi requires the ATPase Cdc48 and cofactor Ufd1 for activation of sterol regulatory element-binding protein in fission yeast. *J. Biol. Chem.* **292**, 16333–16350
25. Fleig, L., Bergbold, N., Sahasrabudhe, P., Geiger, B., Kaltak, L., and Lemberg, M. K. (2012) Ubiquitin-dependent intramembrane rhomboid protease promotes ERAD of membrane proteins. *Mol. Cell* **47**, 558–569
26. Tang, W. K., and Xia, D. (2016) Role of the D1-D2 linker of human VCP/p97 in the asymmetry and ATPase activity of the D1-domain. *Sci. Rep.* **6**, 20037
27. Noguchi, M., Takata, T., Kimura, Y., Manno, A., Murakami, K., Koike, M., Ohizumi, H., Hori, S., and Kakizuka, A. (2005) ATPase activity of p97/valosin-containing protein is regulated by oxidative modification of the evolutionally conserved cysteine 522 residue in Walker A motif. *J. Biol. Chem.* **280**, 41332–41341
28. Higuchi, N., Kato, M., Shundo, Y., Tajiri, H., Tanaka, M., Yamashita, N., Kohjima, M., Kotoh, K., Nakamura, M., Takayanagi, R., and Enjoji, M. (2008) Liver X receptor in cooperation with SREBP-1c is a major lipid synthesis regulator in nonalcoholic fatty liver disease. *Hepatol. Res.* **38**, 1122–1129
29. [preprint] Han, S., Nakakuki, M., Nakagawa, Y., Wang, Y., Araki, M., Yamamoto, Y., Tokiwa, H., Takeda, H., Mizunoe, Y., Motomura, K., Ohno, H., Murayama, Y., Aita, Y., Takeuchi, Y., Osaki, Y., et al. (2021) Rhomboid protease RHBDL4/RHBDD1 cleaves SREBP-1c at ER monitoring and regulating fatty acids. *bioRxiv*. <https://doi.org/10.1101/457590>
30. Tong, Z., Kim, M. S., Pandey, A., and Espenshade, P. J. (2014) Identification of candidate substrates for the Golgi Tull1 E3 ligase using quantitative diGly proteomics in yeast. *Mol. Cell Proteomics* **13**, 2871–2882
31. Liu, T. F., Tang, J. J., Li, P. S., Shen, Y., Li, J. G., Miao, H. H., Li, B. L., and Song, B. L. (2012) Ablation of gp78 in liver improves hyperlipidemia and insulin resistance by inhibiting SREBP to decrease lipid biosynthesis. *Cell Metab.* **16**, 213–225
32. Wei, J., Yuan, Y., Chen, L., Xu, Y., Zhang, Y., Wang, Y., Yang, Y., Peek, C. B., Diebold, L., Yang, Y., Gao, B., Jin, C., Melo-Cardenas, J., Chandel, N. S., Zhang, D. D., et al. (2018) ER-associated ubiquitin ligase HRD1 programs liver metabolism by targeting multiple metabolic enzymes. *Nat. Commun.* **9**, 3659

33. Ye, J., Rawson, R. B., Komuro, R., Chen, X., Davé, U. P., Prywes, R., Brown, M. S., and Goldstein, J. L. (2000) ER stress induces cleavage of membrane-bound ATF6 by the same proteases that process SREBPs. *Mol. Cell* **6**, 1355–1364
34. Lee, J. J., Park, J. K., Jeong, J., Jeon, H., Yoon, J. B., Kim, E. E., and Lee, K. J. (2013) Complex of Fas-associated factor 1 (FAF1) with valosin-containing protein (VCP)-Npl4-Ufd1 and polyubiquitinated proteins promotes endoplasmic reticulum-associated degradation (ERAD). *J. Biol. Chem.* **288**, 6998–7011
35. Tang, W. K., Li, D., Li, C. C., Esser, L., Dai, R., Guo, L., and Xia, D. (2010) A novel ATP-dependent conformation in p97 N-D1 fragment revealed by crystal structures of disease-related mutants. *EMBO J.* **29**, 2217–2229
36. Zhang, X., Gui, L., Zhang, X., Bulfer, S. L., Sanghez, V., Wong, D. E., Lee, Y., Lehmann, L., Lee, J. S., Shih, P. Y., Lin, H. J., Iacovino, M., Weihl, C. C., Arkin, M. R., Wang, Y., *et al.* (2015) Altered cofactor regulation with disease-associated p97/VCP mutations. *Proc. Natl. Acad. Sci. U. S. A.* **112**, E1705–E1714
37. Kuriyama, H., Liang, G., Engelking, L. J., Horton, J. D., Goldstein, J. L., and Brown, M. S. (2005) Compensatory increase in fatty acid synthesis in adipose tissue of mice with conditional deficiency of SCAP in liver. *Cell Metab.* **1**, 41–51